H_2O_2-responsive nanocarriers prepared by RAFT-mediated Polymerization-Induced Self-Assembly of N-(2-(methylthio)ethyl)acrylamide for biomedical applications

Hien Phan,[a] *Robert Cavanagh,*[b] *Damien Destouches,*[c] *Vincenzo Taresco,*[d] *Francis Vacherot,* [c] *Blandine Brissault,*[a] *Jacques Penelle,* [a] *Benoit Couturaud* [a, *]

[a] Institut de Chimie et des Matériaux Paris-Est, Université de Paris-Est Créteil, CNRS UMR 7182, 2 rue Henri Dunant, 94320 Thiais, France

[b] School of Medicine, University of Nottingham, University Park, Nottingham NG7 2RD, UK

[c] Univ Paris Est Créteil, TRePCa, F-94010 Créteil, France

[d] School of Chemistry, University of Nottingham, University Park, Nottingham NG7 2RD, UK

* Corresponding author: benoit.couturaud@cnrs.fr

Keywords: polymer-based nanomedicine, polymerization-induced self-assembly (PISA), reactive oxygen species (ROS), hydrogen peroxide (H_2O_2), responsive nanoparticles, drug delivery

Abstract

H_2O_2-sensitive block copolymer nanoparticles (NPs) composed of a hydrophilic macro-chain transfer agent (macro-CTA) and a hydrophobic thioether-bearing block were prepared by polymerization-induced self-assembly (PISA) approach. PISA process first involved a chain extension of poly((poly(ethylene glycol) methyl ether methacrylate)-*co*-(poly(ethylene glycol) methacrylate)) macro-CTA with a H_2O_2-responsive N-(2-(methylthio)ethyl)acrylamide monomer (MTEAM), which self-assembled into P(PEGMA-*co*-PEGMAOH)-*b*-PMTEAM block copolymer NPs. The polymerization kinetics indicated the evolution of particle size and morphology from spherical micelles, fused micelles, to vesicles over time. Upon incubation with 0.1 to 10 mM H_2O_2, spheres were fragmented due to the oxidation of the PMTEAM cores, thus transforming the hydrophobic thioethers into hydrophilic sulfoxides, and disassociating the nanocarriers. 43 % of the hydrophobic Nile Red dye was encapsulated into the spherical micelles and demonstrated a controlled release in H_2O_2 incubation. Spherical micelles and vesicles displayed no cytotoxicity in MCF-7, DU145 and 22Rv1 cells. Both spheres and vesicles were efficiently internalized into MCF-7 cells, with spheres showing higher level of uptake than vesicles due to the smaller sizes. In summary, PISA of P(PEGMA-*co*-PEGMAOH)-*b*-PMTEAM allowed the direct formation and loading of hydrophobic dye into spherical micelles which showed a controlled drug release in H_2O_2.

1. Introduction

It is becoming increasingly apparent that block copolymer nanocarriers are of great benefit to drug delivery designs and innovative biomaterials applications in a range of therapeutic areas.[1–3] The versatility of block chemistries enables their final supra-macromolecular architectures to be finely tuned, while their amphiphilic balances can be adjusted to exert appropriate stability and colloidal properties.[4,5] Block copolymer NPs are traditionally prepared by nanoprecipitation or thin film hydration methods which usually face several limitations such as low polymer concentrations used (< 1wt%) and multiple intermediate steps.[6] To address these challenges, a promising alternative known as polymerization-induced self-assembly (PISA) has been introduced, since the polymerization of block copolymers and their self-assemblies into NPs are directly obtained in one pot.[7–11] PISA reaction can be implemented by using free radical living polymerization methods, in which reversible addition−fragmentation chain transfer (RAFT) is one of the most widely used approaches, owing to multiple choices of monomer groups and versatile reaction modalities.[12–16] Moreover, a few emerging types of non-radical polymerizations can also be used in PISA, e.g., living anionic polymerization,[17,18] ring opening polymerization (ROP),[19,20] or ring-opening metathesis polymerization PISA (ROMPISA).[21–23] In addition to the facile synthetic route, PISA elicits possibility of achieving morphological evolutions, with spherical micelles initially formed, then cylinders, to higher-ordered vesicles obtained at very high concentration (to 50 wt%) during the polymerization process.[24–30] Thereby, PISA can be a potential formulation alternative over conventional methods to accelerate the commercialization with low manufacture cost and high batch reproducibility.

Together with the emergence of many novel and promising drug molecules, increased concerns are being placed upon developing drug delivery systems that can facilitate high access of bio-

active agents to diseased areas. This is because following systemic administration, therapeutic molecules are likely to face premature plasma degradation and non-specific biodistribution, thus limiting their access and accumulation at the targeted cells. This is particularly true for anti-cancer drugs, which are usually cytotoxic to both healthy and tumor cells, resulting in many severe off-target side effects. Therefore, to maximize treatment outcomes biomolecules should be protected and stabilized within drug delivery carriers during blood circulation, while being selectively released upon reaching targeted tissues. In this regard, the designed drug delivery systems should be able to sense the differences in their surrounding environments and specifically respond to pathological signals, thus programing their drug release profiles as appropriate.[31–35] Meanwhile, disease cells are distinct from healthy cells due to the presence of certain abnormal signals or the imbalance between biological molecules, hence disturbing the physiological mechanisms of cell metabolism and cell survival. One widely known phenomenon is the abnormal increase of reactive oxygen species (ROS) which induces oxidative stress and cell disruption, thus causing a variety of diseases such as cancer, diabetes, infections, and neurodegenerative diseases.[36–38] ROS are free-radical by-products of oxygen metabolism during cell regulation process, which plays a beneficial role in maintaining normal cellular activities at a concentration of 3-10 μM but promotes cellular dysregulation and diseases at 100 μM.[39] Such property has largely been exploited to design nano-vehicles encoded with functionalities sensitive to the increased ROS, inducing molecular structural transitions or disassociation into sub-units to release internal payloads at targeted sites.[40–48] In the context of ROS-responsive drug delivery systems, block copolymer NPs bearing thioether moieties have been widely studied in recent reports, since the hydrophobic thioether incorporated in the water-insoluble segments could be transformed into hydrophilic sulfoxides in the presence

of oxidation species such as H_2O_2, promoting a solubility transition and disrupting the amphiphilic balance to ultimately disassociating block copolymers NPs to releasing their payloads.[49–61]

Taking advantage of the one-step PISA formulation technique while integrating the oxidation-sensitive thioethers into PISA-made nano-assemblies for controlled drug release, we aim to firstly synthesize an acrylate-based H_2O_2-responsive thioether monomer, N-(2-(methylthio)ethyl)acrylamide, which can be polymerized onto a poly(ethylene glycol) methacrylate macro-chain transfer agent (macro-CTA) via the aqueous dispersion RAFT-mediated PISA process to form NPs at 10 wt%. Although PISA has been employed to develop various systems of stimuli-responsive NPs, these methods usually involve the use of pro-drug nanocarriers which requires exhaustive chemical modifications and laborious purifications. This study thus features the *in situ* preparation of H_2O_2-responsive NPs in one pot at high solid contents and investigates the stability of the obtained particle morphologies in bio-mimicking environments, both under physiological and tumor-associated elevated H_2O_2 conditions. Nile Red dye was employed as a hydrophobic drug model to be loaded into the hydrophobic core of spherical micelles during PISA and the study of drug release in H_2O_2 was undertaken. The impacts of particle shapes on their biocompatibilities and cell uptake were also assessed on MCF-7 breast cancer cells.

2. Materials and Methods

2.1. Materials

All chemicals were used as obtained without further purification unless otherwise stated. Poly(ethylene glycol) methyl ether methacrylate M_n = 500 g mol^{-1} (denoted as PEGMA500) (> 95 %, Aldrich) and poly(ethylene glycol) methacrylate M_n = 360 g mol^{-1} (denoted as PEGMAOH) (>

95 %, Aldrich) were activated by aluminum oxide column before use. 4-Cyano-4-(((ethylthio)carbonothioyl)thio)pentanoic acid (CEPA) chain transfer agent (CTA) was synthesized according to the established protocol.[62] Chemical has been sourced as followed : 2,2'-Azobis(2-methylpropionamidine) dihydrochloride azo initiator (V-50, MW = 271.19 g mol^{-1}, Aldrich), 2-(methylthio)ethylamine (95%, Thermo Scientific), 1,4-dioxane (anhydrous ≥ 99.9%, Aldrich), acryloyl chloride (≥ 97 %, Aldrich), triethylamine (TEA, 99 %, Aldrich), phosphate buffered saline (PBS, Aldrich), bovine serum albumin (BSA, Thermo Fisher Scientific), Dulbecco's Modified Eagle Medium (DMEM, Thermo Fisher Scientific), fetal calf serum (FBS, Sigma-Aldrich), RPMI (Invitrogen), Triton X-100 (Aldrich), diamidino-2-phenylindole (DAPI, Aldrich), lysotracker green DND-26 (Thermo-Fisher), Hoechst 33342 (Thermo-Fisher), PrestoBlue cell viability assay (Thermo Fisher Scientific), L-glutamine (Sigma-Aldrich), Sulfo-Cy5 NHS (Lumiprobe). MCF-7 human breast adenocarcinoma cells were obtained from the American Type Culture Collection (Manassas, Virginia) and used in a passage window of 10. DU145 and 22Rv1 human prostate cancer cells and PNT2 non-tumor human cells were obtained from LGC Promochem (Molsheim, France).

2.2. Methods

2.2.1. Synthesis of ROS-sensitive monomer N-(2-(methylthio)ethyl)acrylamide (MTEAM)

1.0 g (11.1 mmol, 1.0 mL) 2-(methylthio)ethylamine was added to a round bottom flask containing 50 mL dry THF and cooled to 0 °C. 1.1 g (11.1 mmol, 1.5 mL) triethylamine was then added to the solution and left to stir for 10 min. 0.1 g (11.1 mol, 0.9 mL) acryloyl chloride was added dropwise and the solution was allowed to warm to room temperature. After 12 h, the white precipitate was filtered and the THF was removed under reduced pressure. The crude mixture was

dissolved in 50 mL of DCM and washed with saturated $NaHCO_3$ (2 x 50 mL) and brine (50 mL). The organic layer was dried over anhydrous $MgSO_4$, filtered, and the solvent was evaporated in a rotavapor. The obtained oil was purified by column chromatography on silica gels using initially 100 % cyclohexane, then cyclohexane:dichloromethane = 50:50 (v/v) and slowly to dichloromethane:methanol = 98:2 (v/v), resulting in the colorless oil at 80.5 % yield.

2.2.2. Synthesis of hydrophilic P(PEGMA-*co*-PEGMAOH) macro-CTA

The chain transfer agent 2-cyano-5-((4-fluorophenyl)amino)-5-oxopentan-2-yl ethyl carbonotrithioate (CEPA CTA) was synthesized according to previous procedure.[62] P(PEGMA-*co*-PEGMAOH) macro-CTA (abbreviated as P) was prepared by RAFT polymerization with two monomers, PEGMA and PEGMAOH in the presence of CEPA CTA, initiated by AIBN at 80 °C in dioxane at a molar ratio of PEGMA:PEGMAOH:CEPA:AIBN = 90:10:1:0.2. The total concentration of two monomers in the solution was 0.5 mol L^{-1}. To begin with, 7.3 mg CEPA (27.8 µmol), 1.25 g PEGMA (2.5 mmol, 1.16 mL), 0.1 g PEGMAOH (278 µmol, 90.5 µL) and 912 µg AIBN (5.6 µmol) were added to an 8-mL glass vial and dissolved in 5.56 mL of dioxane. The vial was sealed and degassed under argon for 30 min and placed in a pre-heated oil bath at 80 °C. 100 µL sample was withdrawn periodically at predetermined time to determine the monomer conversion (%) according to ^1H NMR ($CDCl_3$) and molecular weight distribution and dispersity according to SEC (PMMA standard, DMF). On the ^1H NMR ($CDCl_3$) spectra, the integration of the peak belonging to the methyl groups ($-CH_3$) of PEGMA was fixed at 3 due to the 3 protons at different time points to observe changes of the proton peaks representing the methyl groups ($-CH_2$) of acrylate functions of PEGMA500 and PEGOH360 at 5.5 ppm or 6.1 ppm, with reference to such at t = 0 min. The monomer conversion is thus presented as:

Monomer conversion (%) = $\frac{I_t - I_0}{I_0} x\ 100$ in which I_t and I_0 are integrals at time t and t = 0, respectively.

For SEC, 30 µL of the withdrawn samples were dried under the fume food overnight to evaporate the solvent dioxane and dissolved in 1.5 mL filtered dimethylformamide (DMF), followed by filtering through polytetrafluoroethylene (PTFE) membranes with pore sizes of 0.45 µm to eliminate impurities and bacteria, before subjecting to SEC with poly(methyl methacrylate) (PMMA) standard.

2.2.3. Polymerization-induced self-assembly (PISA) of MTEAM monomer and P(PEGMA-*co*-PEGMAOH) macro-CTA

MTEAM monomer (denoted as M), P(PEGMA-*co*-PEGMAOH) macro-CTA (denoted as P), and V-50 were added into a glass vial at a molar ratio of M:P:V-50 = 300:1:0.2 in deionized water. 80 mg P (2.1 µmol), 93 mg M (641 µmol), and 116 µg V-50 (0.4 µmol) were added to an 8-mL vial and dissolved in 1.73 mL water to obtain a total polymer concentration of 0.1 g mL^{-1} (10 wt%). This vial was degassed under argon for 30 min and placed in a pre-heated oil bath at 60 °C. 100 µL sample was withdrawn at predetermined time intervals using a deoxygenated syringe to study the polymerization kinetics using ^{1}H NMR (DMSO), SEC (PMMA standard, DMF) and TEM.

2.2.4. Colloidal stability in biological media

The stability was undertaken by treating spherical and vesicle solutions with bovine serum albumin (BSA) 0.2 wt% and cell culture medium (DMEM) at 37 °C. The first step involved the preparation of stock solutions of NPs at 2 mg mL^{-1} and of BSA at 2 mg mL^{-1}. 500 µL NPs (2 mg mL^{-1}) were added to a 1.5 mL-Eppendorf and mixed with the BSA solution prepared above (2 mg mL^{-1}) to

produce the final solution containing 1 mg mL^{-1} NPs and 1 mg mL^{-1} BSA. To another Eppendorf, 500 µL NPs (2 mg mL^{-1}) was reacted with 500 µL DMEM. NPs at 1 mg mL^{-1} in PBS were used as a control. Three samples of spherical micelles (in PBS, BSA, DMEM) and three samples under similar conditions of vesicles were incubated in a water bath at 37 °C for 24 h.

2.2.5. Oxidation in H_2O_2

The stock solution of H_2O_2 was prepared at 0.1 M by diluting 10 µL H_2O_2 9.8 M (the commercial product's original concentration) in 990 µL PBS. From this mother solution several H_2O_2 concentrations were prepared at 20 mM, 2 mM, 0.2 mM and 20 µM in PBS. Stock solutions of spheres or vesicles were prepared at 2 mg mL^{-1}. 500 µL NPs (2 mg mL^{-1}) were treated with 500 µL of different H_2O_2 concentrations including 20 mM, 2 mM, 0.2 mM or 20 µM in different Eppendorfs, resulting in final mixture solutions of 1 mg mL^{-1} NPs with 10 mM, 1 mM, 0.1 mM or 10 µM H_2O_2, respectively. These samples were placed in a water bath at 37 °C for 48 h and their sizes and zeta potentials were assessed at predetermined times.

2.2.6. Encapsulation and release study of Nile Red

Nile Red (NR) dye was loaded into the hydrophobic core of the spherical micelles during PISA at a ratio of NR/MTEAM/ P(PEGMA-*co*-PEGMAOH)/V-50 = 0.05/45/1/0.4 with 10 wt% of total solid contents. Briefly, stock solution of NR was prepared at 1 mg mL^{-1} in chloroform. 18 µL of this solution was taken into a 1-mL vial and dried under reduced pressure to remove the chloroform. 5.24 µg MTEAM monomer was then added to the dried NR and mix well until a homogenous solution was achieved. The mixture of NR and MTEAM monomer was added to another vial containing 0.03 g P(PEGMA-*co*-PEGMAOH) macro-CTA in 344 µL deionized H_2O. 8.7 µL of V-50 was taken from a stock solution of V-50 of 0.01 g mL^{-1} and added to the PISA

reaction mixture above. The sample was degassed for 30 min under argon and placed in a pre-heated oil bath at 60 °C for 4 h. The PISA was quenched by exposing the reaction mixture to air and assessed in ^{1}H NMR and DLS. The reaction mixture was centrifuged at 60000 rpm for 4 h at room temperature, and that free NR in water tended to precipitate to the bottom of the vial and the supernatant containing NR-loaded micelles was collected for quantification of drug loading and drug release study.

i) Quantification of drug loading (DL) and encapsulation efficiency (EE)

The solution of NR-loaded NP was freeze-dried overnight, and the obtained solid was dissolved in an appropriate volume of DMSO to measure the UV-Vis absorbance of NR at 550 nm. This data was compared with a known calibration curve of NR in DMSO to calculate the drug loading and encapsulation efficiency, as follows:

$$\text{DL (\%)} = \frac{Amount\ of\ drug\ loaded}{Amount\ of\ solid\ contents}\ x\ 100$$

$$\text{EE (\%)} = \frac{Amount\ of\ drug\ loaded}{Amount\ of\ drug\ initially\ added}\ x\ 100$$

ii) Drug release in H_2O_2

40 µL of the NR-loaded NP dispersion was diluted with 460 µL deionized H_2O in a 1-mL quartz cuvette, obtaining a NP concentration of 8 mg mL^{-1}. 500 µL of H_2O_2 20 mM was added to this mixture, resulting in a particle concentration of 4 mg mL^{-1} and H_2O_2 of 10 mM. 4 mg mL^{-1} of NR-loaded particles in PBS was used as a control. The cuvette was placed in a UV-Vis machine and scanned from 200 – 800 nm every 1 h at 37 °C to observe changes in the spectra over the course of H_2O_2 oxidation.

2.2.7. Attachment of Cy5

Both spheres (P-*b*-M_{45}) and vesicles (P-b-M_{300}) have the hydroxyl functions of PEGMAOH exposed on the surfaces that were used to conjugate with the activated N-hydroxysuccinimide (NHS) ester function of sulfo-cyanine5 NHS ester at a molar ratio of 1:0.1. 900 µL P-b-M_{300} (1.1 µmol) and 86.5 µL sulfo-cyanine5 NHS ester (0.11 µmol) were added into a 5-mL vial and stirred under the fume hood for 24 h. The solution was then dialyzed against deionized water (MWCO 6 - 8 kDa) for 48 h to remove free Cy5. The obtained mixture was lyophilized and then dissolved in an appropriate volume of deionized water to measure the absorbance in UV-Vis at 646 nm. Comparing the absorbance value recorded with the prepared calibration curve of Cy5 in H_2O enabled the quantification of the attached Cy5 and the conjugation yield.

2.2.8. Cell culture

Cell viability and uptake of two NP dispersions of spheres and vesicles were assessed in cancer and normal cell lines, including MCF-7 human breast adenocarcinoma cells, DU145 and 22Rv1 human prostate cancer cells and PNT2 non-tumor human cells. MCF-7 cells were cultured in phenol red free DMEM supplemented with 10 % (v/v) fetal calf serum (FBS) and 2 mM L-glutamine (complete DMEM). DU145, 22RV1, and PNT2 cells were cultured in RPMI supplemented with 10 % FBS. Cells were incubated under humidified atmosphere at 37 °C with 5% CO_2.

Cytocompatibility evaluation

The PrestoBlue™ cell viability assay was carried out to evaluate the cytotoxicity of spheres and vesicles in MCF-7 cells, by following the protocol established in previous literature.[63] MCF-7 cells

were seeded in a 96-well plate with a density of $1x10^4$ cells per well in 100 µL of complete DMEM and incubated for 24 h prior to sample addition. Cells were incubated for 24 h in a fresh complete DMEM containing samples at designed concentrations: 0.005 – 1 mg mL^{-1} (equivalent NP concentration). Three parallel wells were set for each concentration and three individual experiments were carried out. The next steps were explained in the cited work.[63]

Cell viability was studied using MTT assay for spheres and vesicles in two human prostate cancer cell lines, DU145 and 22Rv1, as well as non-tumor human prostate cell line, PNT2. Cells were seeded at a density of 1×10^4 cells per well in 100 µL of the complete medium into a 96-well plate and incubated for 24 h before treatment. NPs were added and incubated for 72 h in a fresh complete medium. MTT (1 mg mL^{-1}) was then added into each well and incubated further for 2 h. Cells were washed twice in PBS and the produced formazan was solubilized in 100 µL of isopropanol. The absorbance of MTT assay was measured at 595 nm.

Fluorescent live cell microscopy

This experiment was to assess the cellular uptake of spheres and vesicles at 250 µg mL^{-1} in MCF-7 cells. Procedures were described in detail in a previously published report.[63]

Fluorometric-based uptake assessment

To further investigate cellular uptake, quantitative kinetic uptake experiments was performed.[63–65] MCF-7 cells were seeded at a density of $1.2x10^5$ cells per well in a 12-well plate and cultured for 48 h. Culture medium was then removed and 1 mL of 250 µg mL^{-1} spheres-Cy5 and vesicles-Cy5 applied in complete DMEM medium. Further steps following exposure could be found in this cited protocol.[63]

3. Results and Discussion

3.1. Synthesis of ROS-sensitive monomer N-(2-(methylthio)ethyl)acrylamide (MTEAM or M)

MTEAM monomer (M) was prepared through reacting 2-(methylthio)ethylamine with acryloyl chloride and trimethylamine for 12 h. Figure S1A presents the ^{1}H NMR spectrum of MTEAM in $CDCl_3$, showing singlet of 3 protons of methyl group (-CH_3, a), triplets of 2 protons belonging to ethyl moieties (-CH_2-CH_2-, b, c), singlet of 1 proton of amine function (-NH, d), and proton peaks of acrylate group (-H, e, f, g), confirming the successful synthesis of the monomer.

3.2. Synthesis of hydrophilic P(PEGMA-*co*-PEGMAOH) macro-CTA (abbreviated as P)

The RAFT co-polymerization of PEGMA (M_n = 500 g mol^{-1}) and PEGMAOH (M_n = 360 g mol^{-1}) was carried out in the presence of CEPA CTA and AIBN initiator at a molar ratio of PEGMA:PEGMAOH:CEPA:AIBN = 90:10:1:0.2 at 80 °C in dioxane, Figure 1A. The kinetics of the polymerization was thoroughly investigated using ^{1}H NMR ($CDCl_3$) and SEC (DMF, PMMA standard), seen Figure 1B and 1C, respectively. The semilogarithmic plot of monomer conversion as a function of time appears to increase linearly over a polymerization period of 270 min reaching 90 % conversion, Figure 1B. This inferred that the polymerization rate followed a first-order kinetics over the entire reaction and almost no terminations did occur. The SEC chromatograms display an increase in molecular weights over time with characteristic peaks and moderately narrow dispersity of 1.3 – 1.5, suggesting that a reasonable control over the polymerization was obtained with the formation of a well-defined macro-CTA suitable for chain extension as depicted in Figure 1C.

Indeed, it is not possible to assess the relative amount of each monomer, PEGMA or PEGOH in the final copolymers by NMR due to the high similarities in ^{1}H NMR signal patterns for the comonomer units. Given the very high structural resemblances between the two methacrylate monomers and the first-order polymerization kinetics, it can be reasonably expected that the copolymer composition at time t (min) would match those of the initial monomer feed at time t = 0 (min) as the structural difference between the two methacrylate esters is quite minimal (i.e., an OH group instead of a methoxy at the very end of the PEG chains) and is not expected to affect the kinetic copolymerization parameters. Both monomers, PEGMA500 and PEGMAOH360, were initially reacted at a molar ratio of 90:10, effectively yielding copolymer with the same composition. As the SEC results obtained for such copolymers cannot provide more than an estimate of the absolute molecular weights, an alternate approach based on the living character of the RAFT polymerization was used. The final degree of polymerization at full conversion can indeed be obtained from the $[M]_0/[\text{RAFT agent}]_0$ ratio, and the degrees of polymerization at any conversion could be obtained by multiplying the above value by the conversion. To obtain the molecular weight, the degree of polymerization must take into account the composition of the copolymer and the molecular weights of the narrow-size comonomers. For example, if the reaction is quenched at t = 180 min, yielding a 77 % of monomer conversion, thereby, the respective molecular weight M_n of P(PEGMA-*co*-PEGMAOH) (P) can be obtained as follows:

$$M_n = \frac{77\,x\,(500\,x\,90+360x10)}{100} = 37 \text{ kg mol}^{-1}$$

This value of 37 kg mol^{-1}was utilized for calculation in further experiments, but its accuracy has to be considered with caution, with an error that can certainly be expected to be in the 5-10 % range given the several assumptions that had to be made in the calculation.

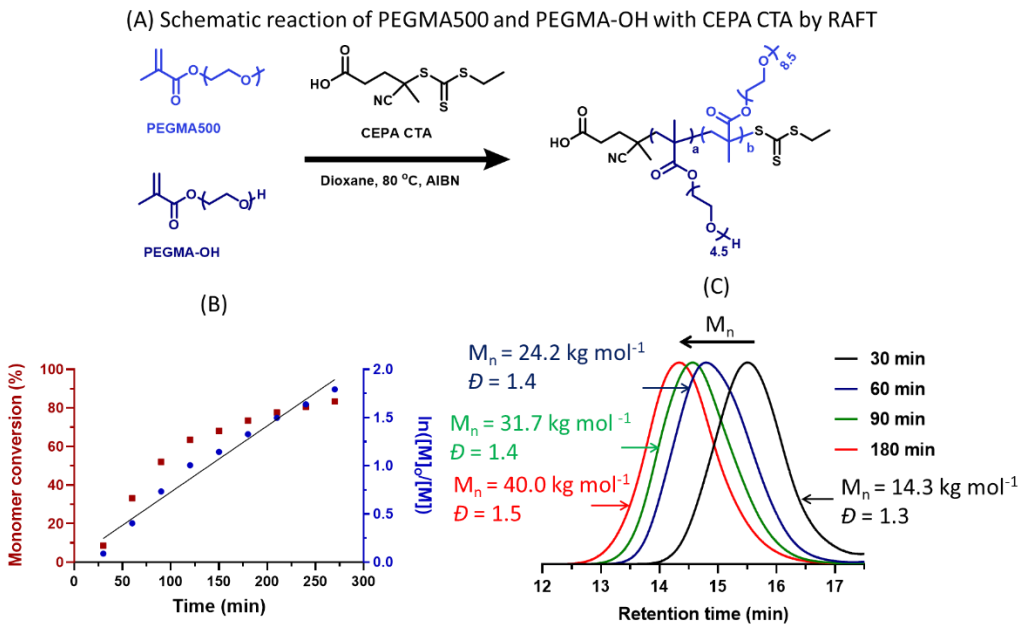

Figure 1. RAFT polymerization of PEGMA and PEGMAOH with CEPA CTA in dioxane at 80 °C and initiated by AIBN. (A) Schematic illustration of the RAFT reaction; (B)-(C) Polymerization kinetics: (B) Monomer conversion % (red square symbol) and semilogarithmic plot (blue circle fitted by linear regression) over time determined by ^{1}H NMR; (C) SEC chromatograms (DMF, PMMA standard) over the reaction period.

3.3. Polymerization-induced self-assembly (PISA) of ROS-sensitive MTEAM monomer (M) and P(PEGMA-*co*-PEGMAOH) macro-CTA (P)

The macro-CTA P(PEGMA-*co*-PEGMAOH) (P) synthesized and characterized above was chain extended with the MTEAM monomer (M) in one-pot PISA using V-50 initiator at 60 °C for 3 h (Figure 2A, Table S1). Figure 2B exhibits three trends, (i) from 0 to 0.75 h, the monomer conversion increases from 5 % to 19 %, (ii) which rises up to 82 % at 1.5 h, and (iii) increases slowly to 100 % toward 3 h. SEC chromatograms show the molecular weight increase during the reaction, Figure 2C. DLS data also indicates the average particle size increases corresponding to

the three different kinetics regimes, from 59 nm at 0.75 h, to 75 nm at 1 h, and 89 nm at 3 h with very low dispersity of 0.13 – 0.24 in all three cases, Figure 2D.

Not only do the particle sizes increase, but their morphologies are also transformed over the three stages of polymerization as indicated above. The morphological transition proceeds as follows: (i) first, spherical micelles are formed at 45 min (Figure 2E1), (ii) these spheres then fused together to form a mixture of spheres and short fused micelles at 1 h (Figure 2E2), which later elongated to longer fused micelles at 1.25 h (Figure 2E3), and (iii) eventually evolve to vesicles at 3 h (Figure 2E4). Table 1 summarizes characteristics of the obtained morphologies. This transitional procedure is in accordance with the general structural changes observed in PISA polymerizations along with the increasing DPs.[11,13,26]

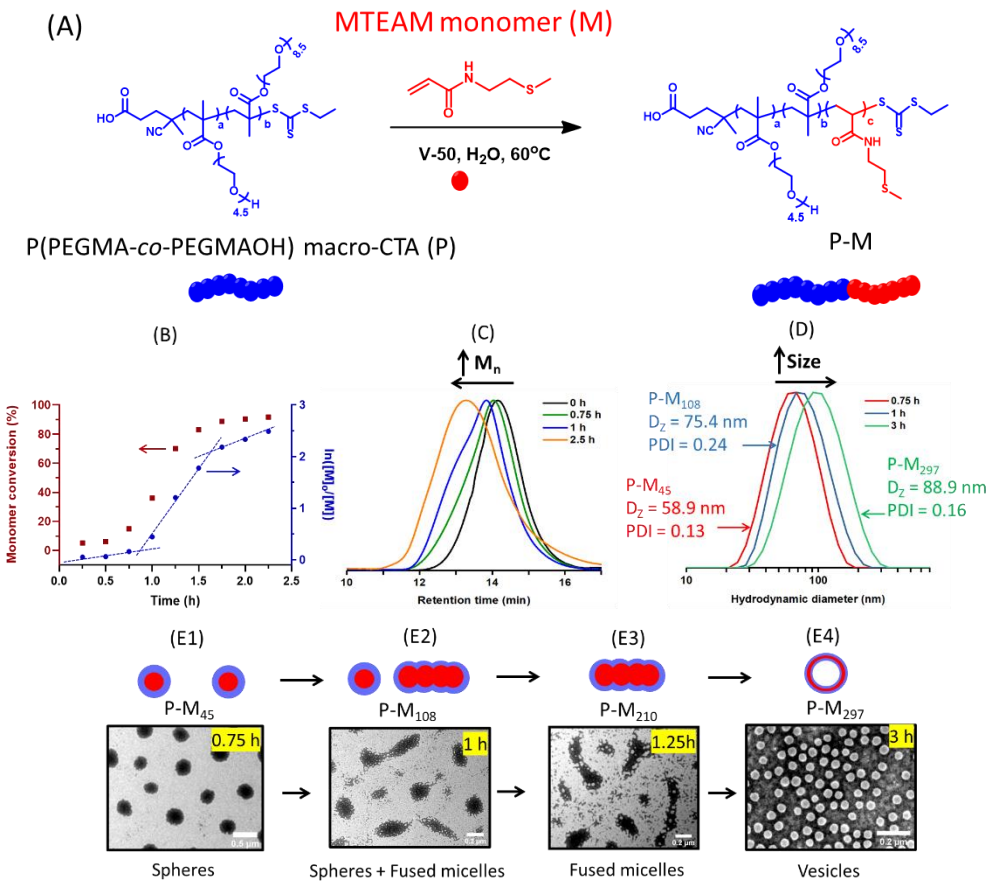

Figure 2. PISA polymerization kinetics of MTEAM monomer (M) by chain extension of P(PEGMA-co-PEGMAOH) macro-CTA (P) in deionized water. (A) Schematic illustration of the reaction; (B) Monomer conversion (%) and semilogarithmic plot over time (h); (C) SEC chromatograms; (D) Normalized intensity of DLS curves; (E) TEM images of particles obtained in the PISA polymerization.

Table 1. Summary of structural features observed for the PISA-made P-M block copolymer NPs

	DP	M_n [a] (kg mol^{-1})	M_n [b] (kg mol^{-1})	$Đ$ [b]	Size [c] (nm)	PDI [c]
Sphere	45	43.9	62.2	1.8	58.9	0.1
Fused micelle	210	67.9	77.7	1.9	80.2	0.1
Vesicle	297	80.6	80.8	2.6	88.9	0.2

[a] Calculated from ^{1}H NMR; [b] SEC (PMMA standard, DMF); *Đ:* Polydispersity (M_w/M_n); [c] DLS

3.4. Colloidal stability in biological media

The colloidal stability studies were undertaken with spherical micelles (Figure 2E1) and vesicles (Figure 2E4), due to their well-defined structures in TEM as compared to the fused micelles that did not provide a clear form of worm-like micelles. Hence, spherical particles (P-M_{45}) and vesicles (P-M_{300}) were incubated in bio-relevant environments, e.g., BSA 0.2 % and DMEM at 37 °C, and their sizes were determined by DLS after 24 h. Figure 3 exhibits that the size distributions of spheres and vesicles in BSA and DMEM remain similar to those of the control NPs in PBS and cause no precipitations. Zeta potentials (ZPs) were recorded, showing the same value of around –10 mV in PBS (control), BSA 0.2 wt%, and DMEM over 24 h (Figure S2). These results indicated a high stability for PISA-made nano-objects under biological conditions.

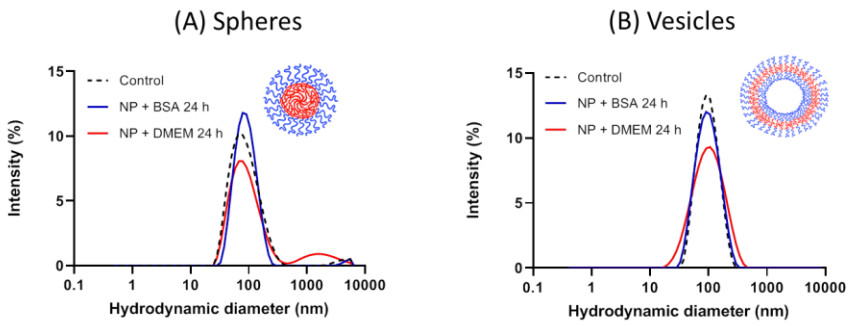

Figure 3. DLS size distributions of (A) spheres and (B) vesicles in BSA and DMEM after 24 h.

3.5. Oxidation in H_2O_2

Spheres (P-M_{45}) and vesicles (P-M_{300}) at 1 mg mL^{-1} were reacted with various concentrations of H_2O_2 at 10 µM, 0.1 mM, 1 mM, and 10 mM at 37 °C.

Initially, spheres treated with 1 mM H_2O_2 showed a decline in size and absolute ZPs over the course of 24 h, with multiple peak distributions starting to appear after 11 h (Figure 4A, Figure 4B), demonstrating that NPs disassociated into small and aggregated pieces upon oxidation. This disruptive process was accelerated when treating the same pristine spherical NPs with 10 mM H_2O_2, resulting in particles quickly crashing out after 2 h. Although the realistic level of H_2O_2 in tumor cells is documented at 0.1 mM, the addition of H_2O_2 0.1 mM to the particle solution induced disassembly relatively late after 48 h, observed from the oxidized signal on ^{1}H NMR (Figure 5). In addition to size and ZP, the particle disruption in H_2O_2 can also be confirmed by observing the derived count rate (kcps) in DLS (Figure 4C), as it correlates with the size and/or concentration of particles in the measured solutions. The optimal count rates should be between 100 and 500 kcps, above which the particle solution is not appropriately diluted or very concentrated while below which particles cannot be detected by DLS's laser, probably due to very small or too diluted NPs. Before any treatment, particle solutions display a count rate of 420 – 450 kcps which falls into the acceptable range (t = 0 h). However, the incubation of 10 mM or 1 mM H_2O_2 caused the count rates to decrease exponentially to less than 100 kcps with no particles being detected after 6 h and 24 h, respectively. Figure 4D shows TEM images of intact spherical particles and aggregates produced from the oxidation after a 24 h treatment with 1 mM H_2O_2. Spherical NPs, after being treated with 1 mM H_2O_2 for 24 h underwent a disruption, which resulted in the formation of smaller aggregates (41 nm), significantly larger PDI (0.4), and a much more diluted dispersion. The fractured small pieces of particles tended to scatter or form larger precipitation, leading to the heterogeneous mixture of small and large aggregates in the TEM image of Figure 4D.

Meanwhile, spheres incubated in 10 μM H_2O_2 mimicking the normal ROS concentration had their sizes unchanged during the treatment period (Figure S3). Together with the good particle stability

in bio-relevant environments illustrated in section 3.4, these results suggest that spherical micelles are stable under physiological conditions, but sensitive to oxidation and prone to be disrupted in H_2O_2.

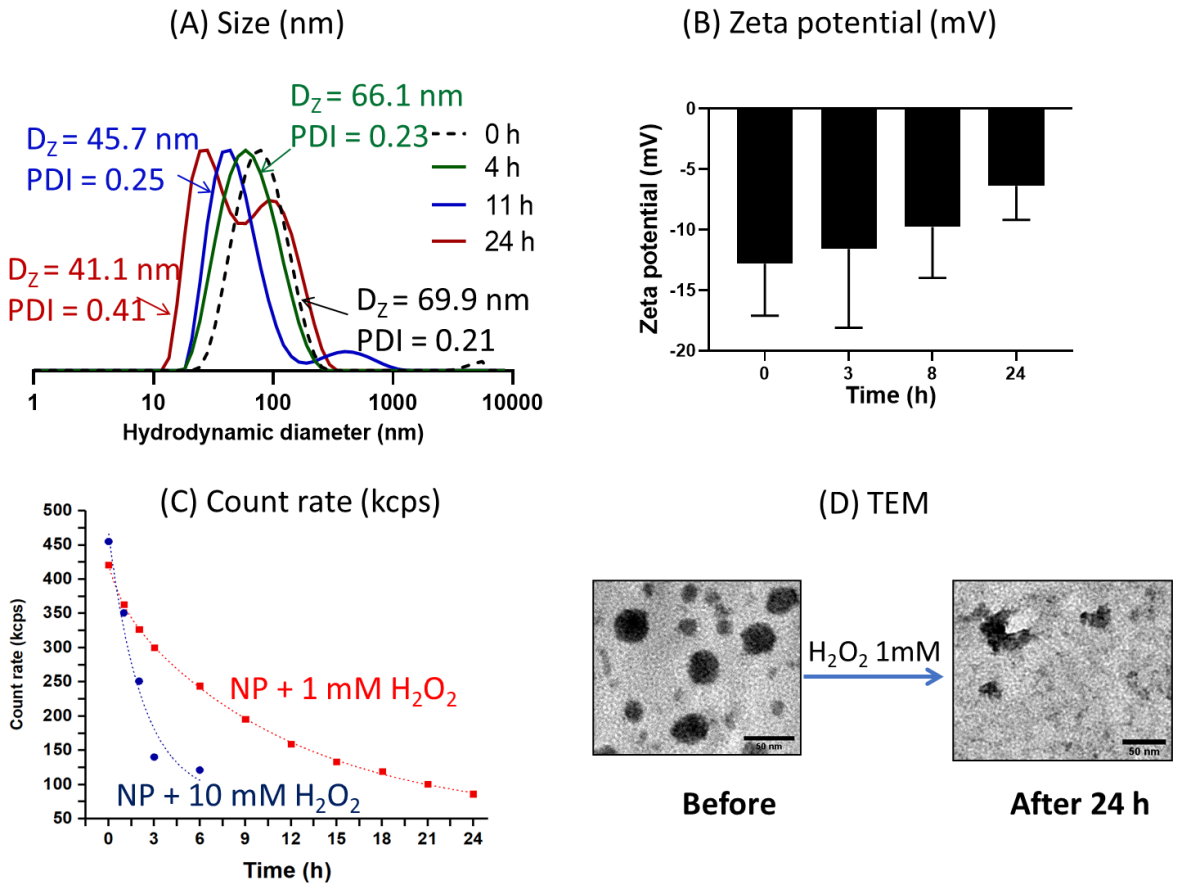

Figure 4. Characterization of spherical micelles of P-M_{45} in 1 mM H_2O_2 during 24 h. (A) Normalized intensity (%) as a function of size (nm) in DLS size distributions; (B) Zeta potential (mV) upon incubation with 1 mM H_2O_2, (C) The exponential decrease of count rates of the same particle solution at 1 mg mL^{-1} when adding 10 mM or 1 mM H_2O_2. Symbols are the experimental points, and the dot lines are fitted with the exponential decay function in Origin 2017. (D) TEM images before and after treatment with 1 mM H_2O_2 in 24 h.

Next, the oxidized solutions at different H_2O_2 concentrations were lyophilized, and the structures of the obtained solids were examined under ^1H NMR (D_2O), Figure 5. The NMR spectrum of spherical NPs oxidized with 10 μM H_2O_2 is similar to such of the initial lone spherical NPs (control) after 24 h of incubation, indicating that spheres are stable at the physiological H_2O_2 concentration of 10 μM. Nonetheless, as the incubating H_2O_2 concentrations increase to 0.1, 1 and 10 mM, the proton peaks of oxidized groups appear with increasing intensities. For example, the NMR spectrum of NPs at 1 mM H_2O_2 illustrates the oxidized signals 1^o and 2^o representing the proton peaks of methyl groups close to the sulfoxide function at 2.7 ppm and 3.1 ppm, respectively. These peaks are relatively weaker for 0.1 mM H_2O_2 but more intense for 10 mM H_2O_2 where the signal 1 (2.2 ppm) completely disappears and is shifted downfield to 1^o (2.7 ppm). The incubation of the MTEAM monomer alone at 10 mM H_2O_2 also exhibits the same chemical shifts of proton peaks of methyl functions adjacent to the sulfoxide (Figure S4), similar to the peak transitions of the oxidized MTEAM block of NPs at 0.1 – 10 mM H_2O_2. The transformation of proton peaks is in agreement with previous studies on ROS-responsive thioether-based polymer systems, thereby confirming that the thioether monomer in the current work was oxidized to sulfoxide at 0.1 mM to 10 mM H_2O_2, thus disrupting the amphiphilic balance of block copolymers and potentially disassociating the spherical structures.[42,66–68]

On the other hand, vesicles (Figure 2E4) were found stable at all tested H_2O_2 concentrations. The TEM image of Figure S5 indicates that the vesicles are slightly swollen after incubating with H_2O_2, which corresponds to an increase in particle sizes from 90 nm to 130 nm (data not shown). The swelling phenomenon is probably attributed to the partial oxidation of the hydrophobic core, and that NPs became slightly more hydrophilic, then water can easily penetrate, thus particles swell and increase in sizes. Despite being partly swollen, vesicles remained stable in H_2O_2, likely due to

the strong hydrogen bonds potentially formed between the hydroxyl functions of PEG and water from two sides of the vesicle membranes, inside toward the hydrophilic core, and outside toward the external surrounding water. Such strong and rigid hydrogen interactions from both surfaces could probably reduce and prevent the penetration of H_2O_2, and that the vesicles were only marginally swollen and still stable. The particle size increase observed following the oxidation process also correlates with previously reported oxidation-sensitive nanomaterials.[51,52,55] Meanwhile spherical micelles are sufficiently stable under normal conditions yet still demonstrate effective responsiveness to H_2O_2, since they only formed hydrogen bonds with the external layer of water, through which the H_2O_2 solutions could permeate more easily to cause the oxidation and the nano-disassembly.

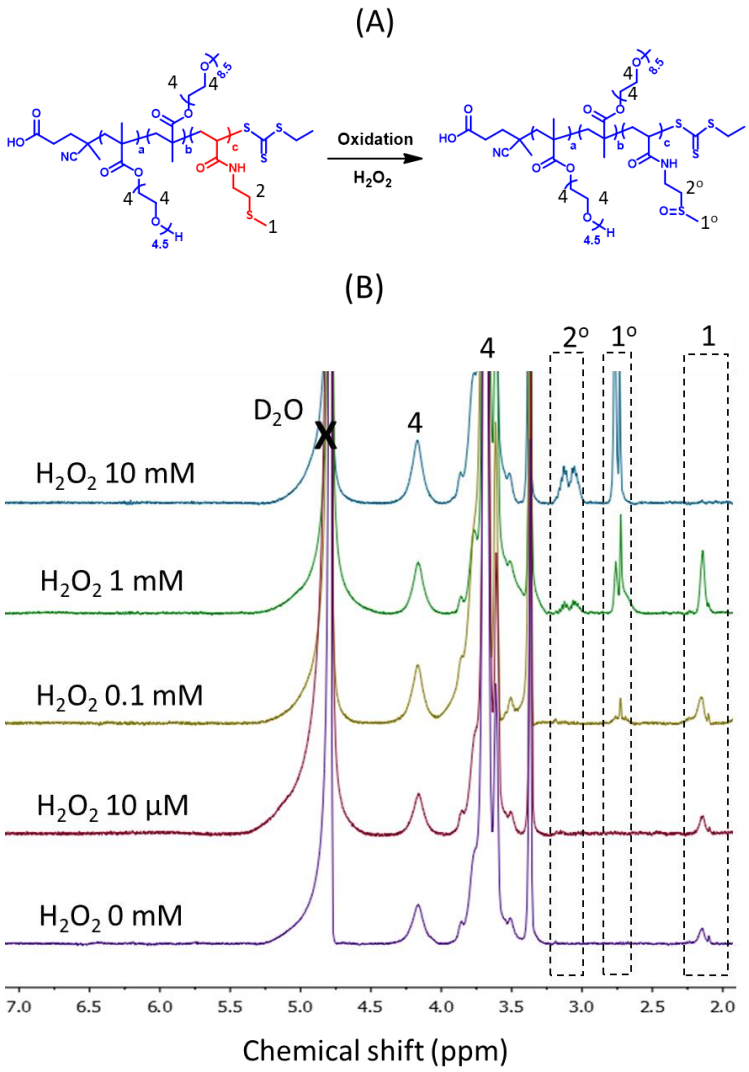

Figure 5. (A) Illustration of oxidative reaction of P-M_{45} block copolymer NPs with H_2O_2; (B) ^1H NMR spectra of P-M_{45} at different concentrations of H_2O_2 in D_2O after 48 h.

3.6 Encapsulation and release of hydrophobic dye Nile Red

The hydrophobic drug model Nile Red (NR) was simultaneously entrapped into the spherical micelles during the PISA with drug loading of 0.03 wt% (compared to the initially theoretical value of 0.05 wt%), and encapsulation efficiency of 43 %. The NR-loaded NPs increased to 78 nm in diameter with PDI of 0.25, with a reference to the plain NPs of 59 nm and PDI of 0.1, indicating

that NR was efficiently entrapped to make such change in size. This was followed by the drug release study of the NR-loaded micelles when exposed to 10 mM H_2O_2. NR is very hydrophobic, highly fluorescent in organic solvents and non-fluorescent in water. Additionally, H_2O_2 does not induce fluorescence-quenching effect on free NR, which has been utilized to assess drug release under oxidation conditions, and to eventually demonstrate that the fluorescence quenching of NR is merely caused by the disruption of NPs and not by H_2O_2.[50,69] Figure 6 shows the spectra of NR-loaded NPs at 10 mM H_2O_2, indicating a reduce in absorbance spectra over time. Although free NR is fluorescent limiting, the loaded NR in an aqueous dispersion can display fluorescence since it is protected in the non-polar core of the NPs. The maximal absorbance of 600 nm is observed at t = 0 h. However, when being exposed for a longer time in H_2O_2, the particles tend to dissociate, free NR is released which shows very limited fluorescence or absorbance in water, thus the amounts of loaded NR decrease and accordingly, their absorbance peaks reduce gradually. Meanwhile, the incubation of NR-loaded NPs in PBS at the same condition did not show any changes in the absorbance spectra, demonstrating the stability of the encapsulated NR in the normal aqueous environment (Figure S6).

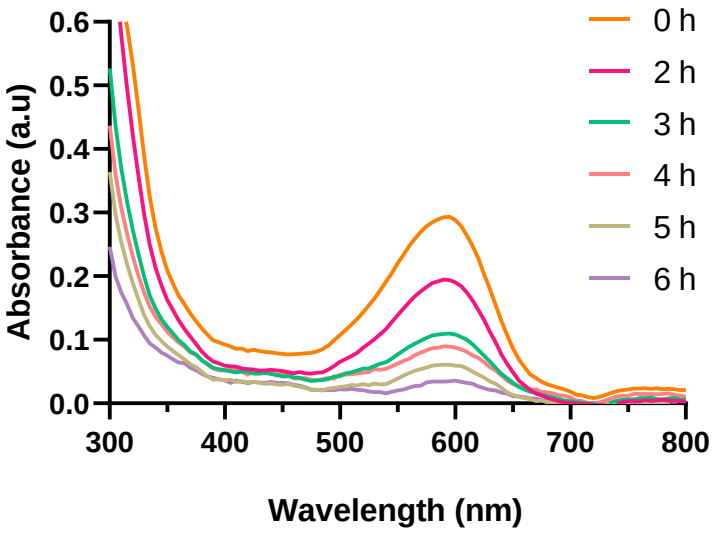

Figure 6. UV-Vis spectra of the NR-loaded NPs as incubated in 10 mM H_2O_2 for 6 h at 37 ºC.

3.7. Attachment of Cy5

Spheres (P-M_{45}) and vesicles (P-M_{300}) were labelled with fluorescent sulfo-cyanine5 NHS ester to facilitate NPs imaging and tracking for biological assessment. This was achieved by functionalizing the hydroxyl end-groups of P(PEGMA-co-PEGMAOH) block with the highly reactive sulfo-NHS ester moieties of Cy5 dye. After a 48 h-dialysis and lyophilization, the obtained solids were resuspended in appropriate volumes of water, and their UV-Vis absorbances were then recorded at 646 nm and compared with the prepared calibration curve of Cy5 in water, resulting in the attached Cy5 concentrations of 48.2 µg mL^{-1} (55.4 % yield) and 69.7 µg mL^{-1} (79.5 % yield) for spheres and vesicles, respectively.

3.8. Cell culture

The Cy5-labelled spheres and vesicles were evaluated in *in vitro* cell culture of MCF-7 breast cancer, and DU145, 22Rv1 prostate cancer cells, and PNT2 non-cancerous cells to observe their effects on cytotoxicity and cell internalization (only implementing on MCF-7) over time.

Cytocompatibility evaluation

The biocompatibility of spheres (P-M_{45}) and vesicles (P-M_{300}) with Cy5 conjugation were assessed in MCF-7 breast cancer cells using the PrestoBlue viability assay (Figure 6), and prostate cells namely DU145 and 22Rv1 (cancer cells) and PNT-2 (non-tumor cells) using the MTT assay (Figure S7, S8). The results display no cytotoxicity on the tested cell lines at all the concentrations investigated up to 1 mg mL^{-1} with approximately 100 % of metabolic activity or cell viability upon incubation. This observation confirmed that the newly synthesized MTEAM monomer and thus

its polymerization into the hydrophobic cores of NPs cause no detrimental effects on the eventual biocompatibility, as well as indicate the absence of toxic residues or solvent traces in the NP dispersions from the synthesis and modification procedures.

Cell uptake

Spheres and vesicles were labelled with Cy5 and incubated with MCF-7 cells for 4 h to assess cell internalization. The confocal microscopy demonstrates the intracellular accumulation and uptake for both NPs, Figure 7C. Spheres and vesicles are shown to co-localize with lysosomes with Pearson's Correlation Coefficient (PCC) values calculated at 0.59 and 0.51 for spheres and vesicles, respectively, indicating potential endocytosis of NPs and trafficking to lysosomal system, Figure 7D.

In addition to observing the intracellular location of NPs, the fluorometric-based uptake kinetics indicates time-dependent uptake of two morphologies and the number of NPs internalized over time. Figure 7B shows that spherical and vesicle NPs display the fastest rate of uptake within the first 60 min. However, this follows different trends afterward in which the uptake of sphere NPs continues to increase rapidly, while vesicles exhibit a very slight increase in cell uptake until 240 min. The differing uptake rates and profiles observed suggest that the spherical and vesicle NPs are internalized via different mechanisms.[70] Moreover, a higher number of spherical micelles were taken up as compared to vesicles at all the timepoints tested. These results implied that 60 nm spherical micelles were internalized more efficiently and imparted higher level of uptake than the 90 nm vesicle NPs. This observation of NP size-dependent uptake reflects reports in the literature that demonstrate increased uptake with smaller NPs.[71–74] This phenomenon has been attributed to NP size-dependent utilization of distinct endocytosis pathways. For example, clathrin-mediated

endocytosis may be available for both sized NPs to exploit, due to clathrin-coated vesicle being in the range of 100-150 nm in diameter.[75,76] However, the caveolin-mediated route may be restricted to only the smaller 60 nm spherical NPs. Caveolin membrane invaginations and vesicles are reported to be < 80 nm in diameter,[75,77] hence limiting internalization of the 90 nm vesicle NPs via this endocytosis pathway. Further study with endocytosis inhibitors would be required to confirm these hypotheses. Nevertheless, the increased uptake observed with spherical NPs indicates that these particles would be the most appropriate as vehicles for drug delivery.

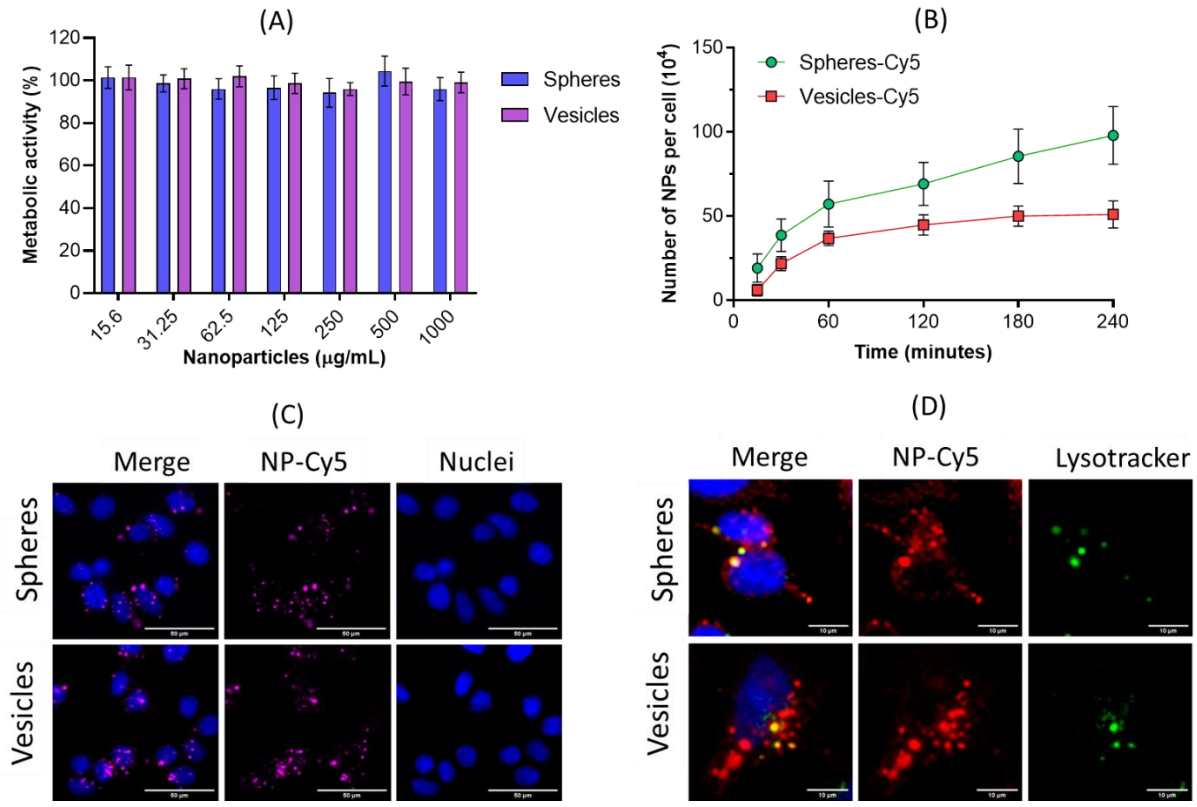

Figure 7. (A) Cytocompatibility of NPs of spheres (P-M_{45}) and vesicles (P-M_{300}) on MCF-7 breast cells after 24-h incubation; (B) Assessment of spheres and vesicles uptake kinetics using fluorometric method; (C) & (D) Uptake characteristics of spheres and vesicles in MCF-7 cells. Cells were incubated with 250 μg mL^{-1} NP solutions for 4 h; (C) Cell nuclei were colored with

Hoechst 33342 (blue), NP-Cy5 (pink). Scale bar = 50 μm; (D) Co-localization in MCF-7 cells. Cy5 signal of NP-Cy5 was false labelled to red to help visualization of co-localization with green lysosomal signal. Merged images are NP-Cy5 signal (red), lysosome stain (green) and Hoechst 33342 staining of nuclei (blue). Scale bar = 10 μm. Images were processed on Image J software. Three individual experiments were carried out for each assay with triplicates for each experiment.

4. Conclusions and Perspectives

H_2O_2-responsive NPs were readily prepared by one-pot PISA polymerization of the oxidation-sensitive MTEAM monomer in the presence of P(PEGMA-*co*-PEGMAOH) macro-CTA in water, showing the increases of molecular weights and particle sizes, along with a morphological transition from spherical micelles, to fused micelles, and vesicles of less than 100 nm over the polymerization kinetics. The spherical micelles prepared from the P-M_{45} block copolymer indicated sufficient stability in physiological environments (BSA 0.2 %wt and DMEM). However, they disassociated upon incubating with 0.1 – 10 mM H_2O_2 solutions, as the thioether functionalities in the hydrophobic core were oxidized into hydrophilic sulfoxides, thus disrupting the amphiphilic balance and ultimately the micellar structures. On the other hand, vesicles or polymersomes of P-M_{300} appeared slightly swollen as being partially oxidized under all the tested H_2O_2 conditions. The hydrophobic dye Nile Red was loaded during PISA at 43 % of encapsulation efficiency and indicated a controlled release of Nile Red over the course of H_2O_2 incubation. Spheres and vesicles were well-tolerated in MCF-7 human breast cancer as well as prostate cells. Both NP shapes were demonstrated to accumulate inside lysosomes in MCF-7 cells which suggested the cell internalization was potentially realized via an endocytosis-mediated pathway, with higher number of spherical NPs being taken up compared to vesicles due to the smaller size.

While the current study succeeded in preparing spherical micelles *in situ*, which were stable in physiological conditions yet disassociated in the increasing H_2O_2 or ROS-rich environments, the remaining challenge is how to achieve vesicles that are also sensitive to high tumorigenic H_2O_2 concentrations when using similar PISA procedure and materials. Therefore, future studies should be investigating the effects of hydrophilic and/or ROS-hydrophobic segments on the disassociation of particles in ROS-rich conditions. Drug molecules could be encapsulated to assess drug release kinetics. Finally, it is noteworthy of studying the behaviors of NPs on other cell lines related to ROS overexpression, e.g., neurodegenerative diseases, and carrying out *in vivo* experiments.

Conflict of interest

The authors declare no conflict of interest.

Supporting Information

Supporting Information is available containing NMR spectra, DLS size distribution curves, and TEM images.

Author information

Corresponding Author

Benoit Couturaud: benoit.couturaud@cnrs.fr

Author Contributions

HP worked on the conceptualization, experimentation, and writing of the original draft. RC and DD contributed to the biological tests and discussion. BB, VT, JP and BC reviewed and edited the current work. All authors have given approval to the final version of the manuscript.

Acknowledgment

HP is financially supported by MESRI scholarship and UPEC for the academic years of 2019-2022. Benoit Couturaud is grateful for the support from DIM RESPORE.

References

(1) Rösler, A.; Vandermeulen, G. W. M.; Klok, H.-A. Advanced Drug Delivery Devices via Self-Assembly of Amphiphilic Block Copolymers. *Adv. Drug Deliv. Rev.* **2012**, *64* (SUPPL.), 270–279.

(2) Adams, M. L.; Lavasanifar, A.; Kwon, G. S. MINIREVIEW Amphiphilic Block Copolymers for Drug Delivery. *Pharm. Assoc. J Pharm Sci* **2003**, *92* (7), 1343–1355.

(3) Taresco, V.; Abelha, T. F.; Cavanagh, R. J.; Vasey, C. E.; Anane-Adjei, A. B.; Pearce, A. K.; Monteiro, P. F.; Spriggs, K. A.; Clarke, P.; Ritchie, A.; Martin, S.; Rahman, R.; Grabowska, A. M.; Ashford, M. B.; Alexander, C. Functionalized Block Co-Polymer Pro-Drug Nanoparticles with Anti-Cancer Efficacy in 3D Spheroids and in an Orthotopic Triple Negative Breast Cancer Model. *Adv. Ther.* **2021**, *4* (1), 2000103.

(4) Vasey, C. E.; Pearce, A. K.; Sodano, F.; Cavanagh, R.; Abelha, T.; Cuzzucoli Crucitti, V.; Anane-Adjei, A. B.; Ashford, M.; Gellert, P.; Taresco, V.; Alexander, C. Amphiphilic Tri- and Tetra-Block Co-Polymers Combining Versatile Functionality with Facile Assembly into Cytocompatible Nanoparticles. *Biomater. Sci.* **2019**, *7* (9), 3832–3845.

(5) Phan, H.; Minut, R. I.; McCrorie, P.; Vasey, C.; Larder, R. R.; Krumins, E.; Marlow, M.; Rahman, R.; Alexander, C.; Taresco, V.; Pearce, A. K. Role of Self-assembly Conditions and Amphiphilic Balance on Nanoparticle Formation of PEG-PDLLA Copolymers in Aqueous Environments. *J. Polym. Sci. Part A Polym. Chem.* **2019**, *57* (17), 1801–1810.

(6) Tyrrell, Z. L.; Shen, Y.; Radosz, M. Fabrication of Micellar Nanoparticles for Drug Delivery through the Self-Assembly of Block Copolymers. *Prog. Polym. Sci.* **2010**, *35* (9), 1128–1143.

(7) Phan, H.; Taresco, V.; Penelle, J.; Couturaud, B. Polymerisation-Induced Self-Assembly

(PISA) as a Straightforward Formulation Strategy for Stimuli-Responsive Drug Delivery Systems and Biomaterials: Recent Advances. *Biomater. Sci.* **2021**, *9* (1), 38–50.

(8) Canning, S. L.; Smith, G. N.; Armes, S. P. A Critical Appraisal of RAFT-Mediated Polymerization-Induced Self-Assembly. *Macromolecules* **2016**, *49* (6), 1985–2001.

(9) Lansalot, M.; Rieger, J. Polymerization-Induced Self-Assembly. *Macromol. Rapid Commun.* **2019**, *40* (2), 1–3.

(10) Foster, J. C.; Varlas, S.; Couturaud, B.; Jones, J. R.; Keogh, R.; Mathers, R. T.; O'Reilly, R. K. Predicting Monomers for Use in Polymerization-Induced Self-Assembly. *Angew. Chemie - Int. Ed.* **2018**, *57* (48), 15733–15737.

(11) Couturaud, B.; Georgiou, P. G.; Varlas, S.; Jones, J. R.; Arno, M. C.; Foster, J. C.; O'Reilly, R. K. Poly(Pentafluorophenyl Methacrylate)-Based Nano-Objects Developed by Photo-PISA as Scaffolds for Post-Polymerization Functionalization. *Macromol. Rapid Commun.* **2019**, *40* (2), 1800460.

(12) Derry, M. J.; Fielding, L. A.; Armes, S. P. Polymerization-Induced Self-Assembly of Block Copolymer Nanoparticles via RAFT Non-Aqueous Dispersion Polymerization. *Prog. Polym. Sci.* **2016**, *52*, 1–18.

(13) Karagoz, B.; Boyer, C.; Davis, T. P. Simultaneous Polymerization-Induced Self-Assembly (PISA) and Guest Molecule Encapsulation. *Macromol. Rapid Commun.* **2014**, *35* (4), 417–421.

(14) Hatton, F. L.; Lovett, J. R.; Armes, S. P. Synthesis of Well-Defined Epoxy-Functional Spherical Nanoparticles by RAFT Aqueous Emulsion Polymerization. *Polym. Chem.* **2017**, *8* (33), 4856–4868.

(15) Siirilä, J.; Häkkinen, S.; Tenhu, H. The Emulsion Polymerization Induced Self-Assembly of a Thermoresponsive Polymer Poly(: N -Vinylcaprolactam). *Polym. Chem.* **2019**, *10* (6), 766–775.

(16) Lesagedelahaye, J.; Zhang, X.; Chaduc, I.; Brunel, F.; Lansalot, M.; D'Agosto, F. The

Effect of Hydrophile Topology in RAFT-Mediated Polymerization-Induced Self-Assembly. *Angew. Chemie - Int. Ed.* **2016**, *55* (11), 3739–3743.

(17) Alegria, A.; Lund, R.; Barroso-Bujans, F.; Arbe, A.; Colmenero, J. Component Dynamics in Nanostructured PI-PDMS Diblock Copolymers with PI Segregated in Lamellas, Cylinders, and Spheres. *Colloid Polym. Sci.* **2014**, *292* (8), 1863–1876.

(18) Wang, X.; Hall, J. E.; Warren, S.; Krom, R.; Magistrelli, J. M.; Rackaitis, M.; Bohm, G. G. A. Synthesis, Characterization, and Application of Novel Polymeric Nanoparticles. *Macromolecules* **2007**, *40* (3), 499–508.

(19) Jiang, J.; Zhang, X.; Fan, Z.; Du, J. Ring-Opening Polymerization of N-Carboxyanhydride-Induced Self-Assembly for Fabricating Biodegradable Polymer Vesicles. *ACS Macro Lett.* **2019**, *8* (10), 1216–1221.

(20) Grazon, C.; Salas-Ambrosio, P.; Antoine, S.; Ibarboure, E.; Sandre, O.; Clulow, A. J.; Boyd, B. J.; Grinstaff, M. W.; Lecommandoux, S.; Bonduelle, C. Aqueous ROPISA of α-Amino Acid: N -Carboxyanhydrides: Polypeptide Block Secondary Structure Controls Nanoparticle Shape Anisotropy. *Polym. Chem.* **2021**, *12* (43), 6242–6251.

(21) Wright, D. B.; Thompson, M. P.; Touve, M. A.; Carlini, A. S.; Gianneschi, N. C. Enzyme-Responsive Polymer Nanoparticles via Ring-Opening Metathesis Polymerization-Induced Self-Assembly. *Macromol. Rapid Commun.* **2019**, *40* (2), 1800467.

(22) Varlas, S.; Foster, J. C.; O'Reilly, R. K. Ring-Opening Metathesis Polymerization-Induced Self-Assembly (ROMPISA). *Chem. Commun.* **2019**, *55* (62), 9066–9071.

(23) Chen, J.; Sun, R.; Liao, X.; Han, H.; Li, Y.; Xie, M. Tandem Metathesis Polymerization-Induced Self-Assembly to Nanostructured Block Copolymer and the Controlled Triazolinedione Modification for Enhancing Dielectric Properties. *Macromolecules* **2018**, *51* (24), 10202–10213.

(24) D'Agosto, F.; Rieger, J.; Lansalot, M. RAFT-Mediated Polymerization-Induced Self-Assembly. *Angew. Chemie Int. Ed.* **2020**, *59* (22), 8368–8392.

(25) Phan, H.; Cossutta, M.; Houppe, C.; Le Cœur, C.; Prevost, S.; Cascone, I.; Courty, J.; Penelle, J.; Couturaud, B. Polymerization-Induced Self-Assembly (PISA) for in Situ Drug Encapsulation or Drug Conjugation in Cancer Application. *J. Colloid Interface Sci.* **2022**, *618*, 173–184.

(26) Zhao, W.; Ta, H. T.; Zhang, C.; Whittaker, A. K. Polymerization-Induced Self-Assembly (PISA) - Control over the Morphology of 19F-Containing Polymeric Nano-Objects for Cell Uptake and Tracking. *Biomacromolecules* **2017**, *18* (4), 1145–1156.

(27) Wang, X.; An, Z. New Insights into RAFT Dispersion Polymerization-Induced Self-Assembly: From Monomer Library, Morphological Control, and Stability to Driving Forces. *Macromol. Rapid Commun.* **2019**, *40* (2), 1800325.

(28) Rieger, J. Guidelines for the Synthesis of Block Copolymer Particles of Various Morphologies by RAFT Dispersion Polymerization. *Macromol. Rapid Commun.* **2015**, *36* (16), 1458–1471.

(29) Hunter, S. J.; Lovett, J. R.; Mykhaylyk, O. O.; Jones, E. R.; Armes, S. P. Synthesis of Diblock Copolymer Spheres, Worms and Vesicles: Via RAFT Aqueous Emulsion Polymerization of Hydroxybutyl Methacrylate. *Polym. Chem.* **2021**, *12* (25), 3629–3639.

(30) Karagoz, B.; Esser, L.; Duong, H. T.; Basuki, J. S.; Boyer, C.; Davis, T. P. Polymerization-Induced Self-Assembly (PISA)-Control over the Morphology of Nanoparticles for Drug Delivery Applications. *Polym. Chem.* **2014**, *5* (2), 350–355.

(31) Taresco, V.; Alexander, C.; Singh, N.; Pearce, A. K. Stimuli-Responsive Prodrug Chemistries for Drug Delivery. *Adv. Ther.* **2018**, *1* (4), 1800030.

(32) Sahle, F. F.; Lowe, T. L. Design Strategies for Programmable Oligonucleotide Nanotherapeutics. *Drug Discov. Today* **2020**, *25* (1), 73–88.

(33) Steele, T. W. J.; Klok, H. A. Stimuli-Sensitive and -Responsive Polymer Biomaterials. *Biomacromolecules* **2018**, *19* (5), 1375–1377.

(34) Cheng, R.; Meng, F.; Deng, C.; Klok, H. A.; Zhong, Z. Dual and Multi-Stimuli Responsive

Polymeric Nanoparticles for Programmed Site-Specific Drug Delivery. *Biomaterials* **2013**, *34* (14), 3647–3657.

(35) Couvreur, P.; Vauthier, C. Nanotechnology: Intelligent Design to Treat Complex Disease. *Pharm. Res.* **2006**, *23* (7), 1417–1450.

(36) Perillo, B.; Di Donato, M.; Pezone, A.; Di Zazzo, E.; Giovannelli, P.; Galasso, G.; Castoria, G.; Migliaccio, A. ROS in Cancer Therapy: The Bright Side of the Moon. *Exp. Mol. Med.* **2020**, *52* (2), 192–203.

(37) Waris, G.; Ahsan, H. Reactive Oxygen Species: Role in the Development of Cancer and Various Chronic Conditions. *J. Carcinog.* **2006**, *5*, 14.

(38) Liou, G.-Y.; Storz, P. Reactive Oxygen Species in Cancer. *Free Radic. Res.* **2010**, *44* (5), 479–496.

(39) Giorgio, M.; Trinei, M.; Migliaccio, E.; Pelicci, P. G. Hydrogen Peroxide: A Metabolic by-Product or a Common Mediator of Ageing Signals? *Nat. Rev. Mol. Cell Biol.* **2007**, *8* (9), 722–728.

(40) Sun, C.; Liang, Y.; Hao, N.; Xu, L.; Cheng, F.; Su, T.; Cao, J.; Gao, W.; Pu, Y.; He, B. A ROS-Responsive Polymeric Micelle with a π-Conjugated Thioketal Moiety for Enhanced Drug Loading and Efficient Drug Delivery. *Org. Biomol. Chem.* **2017**, *15* (43), 9176–9185.

(41) Xu, X.; Saw, P. E.; Tao, W.; Li, Y.; Ji, X.; Bhasin, S.; Liu, Y.; Ayyash, D.; Rasmussen, J.; Huo, M.; Shi, J.; Farokhzad, O. C. ROS-Responsive Polyprodrug Nanoparticles for Triggered Drug Delivery and Effective Cancer Therapy. *Adv. Mater.* **2017**, *29* (33), 1–6.

(42) Wang, G.; Huang, P.; Qi, M.; Li, C.; Fan, W.; Zhou, Y.; Zhang, R.; Huang, W.; Yan, D. Facile Synthesis of a H2O2-Responsive Alternating Copolymer Bearing Thioether Side Groups for Drug Delivery and Controlled Release. *ACS Omega* **2019**, *4* (17), 17600–17606.

(43) Tang, Y.; Ji, Y.; Yi, C.; Cheng, D.; Wang, B.; Fu, Y.; Xu, Y.; Qian, X.; Choonara, Y. E.; Pillay, V.; Zhu, W.; Liu, Y.; Nie, Z. Self-Accelerating H2O2-Responsive Plasmonic Nanovesicles for Synergistic Chemo/Starving Therapy of Tumors. *Theranostics* **2020**, *10*

(19), 8691–8704.

(44) Yang, B.; Chen, Y.; Shi, J. Reactive Oxygen Species (ROS)-Based Nanomedicine. *Chem. Rev.* **2019**, *119* (8), 4881–4985.

(45) Ye, H.; Zhou, Y.; Liu, X.; Chen, Y.; Duan, S.; Zhu, R.; Liu, Y.; Yin, L. Recent Advances on Reactive Oxygen Species-Responsive Delivery and Diagnosis System. *Biomacromolecules* **2019**, *20* (7), 2441–2463.

(46) Kwon, S.; Ko, H.; You, D. G.; Kataoka, K.; Park, J. H. Nanomedicines for Reactive Oxygen Species Mediated Approach: An Emerging Paradigm for Cancer Treatment. *Acc. Chem. Res.* **2019**, *52* (7), 1771–1782.

(47) Lallana, E.; Tirelli, N. Oxidation-Responsive Polymers: Which Groups to Use, How to Make Them, What to Expect from Them (Biomedical Applications). *Macromol. Chem. Phys.* **2013**, *214* (2), 143–158.

(48) El-Mohtadi, F.; D'Arcy, R.; Tirelli, N. Oxidation-Responsive Materials: Biological Rationale, State of the Art, Multiple Responsiveness, and Open Issues. *Macromol. Rapid Commun.* **2019**, *40* (1), 1800699.

(49) Yan, B.; Zhang, Y.; Wei, C.; Xu, Y. Facile Synthesis of ROS-Responsive Biodegradable Main Chain Poly(Carbonate-Thioether) Copolymers. *Polym. Chem.* **2018**, *9* (7), 904–911.

(50) Yoo, J.; Sanoj Rejinold, N.; Lee, D. Y.; Jon, S.; Kim, Y. C. Protease-Activatable Cell-Penetrating Peptide Possessing ROS-Triggered Phase Transition for Enhanced Cancer Therapy. *J. Control. Release* **2017**, *264*, 89–101.

(51) Piergentili, I.; Bouwmans, P. R.; Reinalda, L.; Lewis, R. W.; Klemm, B.; Liu, H.; de Kruijff, R. M.; Denkova, A. G.; Eelkema, R. Thioanisole Ester Based Logic Gate Cascade to Control ROS-Triggered Micellar Degradation. *Polym. Chem.* **2022**, 2383–2390.

(52) Rajes, K.; Walker, K. A.; Hadam, S.; Zabihi, F.; Ibrahim-Bacha, J.; Germer, G.; Patoka, P.; Wassermann, B.; Rancan, F.; Rühl, E.; Vogt, A.; Haag, R. Oxidation-Sensitive Core-Multishell Nanocarriers for the Controlled Delivery of Hydrophobic Drugs. *ACS Biomater.*

Sci. Eng. **2021**, *7* (6), 2485–2495.

(53) Qiao, Z. Y.; Zhao, W. J.; Cong, Y.; Zhang, D.; Hu, Z.; Duan, Z. Y.; Wang, H. Self-Assembled ROS-Sensitive Polymer-Peptide Therapeutics Incorporating Built-in Reporters for Evaluation of Treatment Efficacy. *Biomacromolecules* **2016**, *17* (5), 1643–1652.

(54) Luo, C.; Sun, J.; Liu, D.; Sun, B.; Miao, L.; Musetti, S.; Li, J.; Han, X.; Du, Y.; Li, L.; Huang, L.; He, Z. Self-Assembled Redox Dual-Responsive Prodrug-Nanosystem Formed by Single Thioether-Bridged Paclitaxel-Fatty Acid Conjugate for Cancer Chemotherapy. *Nano Lett.* **2016**, *16* (9), 5401–5408.

(55) Van Der Vlies, A. J.; Xu, J.; Ghasemi, M.; Bator, C.; Bell, A.; Rosoff-Verbit, B.; Liu, B.; Gomez, E. D.; Hasegawa, U. Thioether-Based Polymeric Micelles with Fine-Tuned Oxidation Sensitivities for Chemotherapeutic Drug Delivery. *Biomacromolecules* **2022**, *23* (1), 77–88.

(56) Wang, J.; Li, D.; Tao, W.; Lu, Y.; Yang, X.; Wang, J. Synthesis of an Oxidation-Sensitive Polyphosphoester Bearing Thioether Group for Triggered Drug Release. *Biomacromolecules* **2019**, *20* (4), 1740–1747.

(57) Dong, S.; Liu, L.; Zhao, H. Copper-Coordination Induced Fabrication of Stimuli-Responsive Polymersomes from Amphiphilic Block Copolymer Containing Pendant Thioethers. *Polym. Chem.* **2021**, *12* (21), 3105–3115.

(58) Dong, S.; Jiang, Y.; Qin, G.; Liu, L.; Zhao, H. Methionine-Based PH and Oxidation Dual-Responsive Block Copolymer: Synthesis and Fabrication of Protein Nanogels. *Biomacromolecules* **2020**, *21* (10), 4063–4075.

(59) Duro-Castano, A.; Rodríguez-Arco, L.; Ruiz-Pérez, L.; De Pace, C.; Marchello, G.; Noble-Jesus, C.; Battaglia, G. One-Pot Synthesis of Oxidation-Sensitive Supramolecular Gels and Vesicles. *Biomacromolecules* **2021**, *22* (12), 5052–5064.

(60) Shu, M.; Tang, J.; Chen, L.; Zeng, Q.; Li, C.; Xiao, S.; Jiang, Z.; Liu, J. Tumor Microenvironment Triple-Responsive Nanoparticles Enable Enhanced Tumor Penetration and Synergetic Chemo-Photodynamic Therapy. *Biomaterials* **2021**, *268* (September 2020),

120574.

(61) Song, W.; You, J.; Zhang, Y.; Yang, Q.; Jiao, J.; Zhang, H. Recent Studies on Hydrogels Based on H2O2-Responsive Moieties: Mechanism, Preparation and Application. *Gels* **2022**, *8* (6), 361.

(62) Truong, N. P.; Dussert, M. V.; Whittaker, M. R.; Quinn, J. F.; Davis, T. P. Rapid Synthesis of Ultrahigh Molecular Weight and Low Polydispersity Polystyrene Diblock Copolymers by RAFT-Mediated Emulsion Polymerization. *Polym. Chem.* **2015**, *6* (20), 3865–3874.

(63) Vasey, C. E.; Cavanagh, R. J.; Taresco, V.; Moloney, C.; Smith, S.; Rahman, R.; Alexander, C. Polymer Pro-Drug Nanoparticles for Sustained Release of Cytotoxic Drugs Evaluated in Patient-Derived Glioblastoma Cell Lines and In Situ Gelling Formulations. *Pharmaceutics* **2021**, *13* (2), 208.

(64) Anane-Adjei, A. B.; Fletcher, N. L.; Cavanagh, R. J.; Houston, Z. H.; Crawford, T.; Pearce, A. K.; Taresco, V.; Ritchie, A. A.; Clarke, P.; Grabowska, A. M.; Gellert, P. R.; Ashford, M. B.; Kellam, B.; Thurecht, K. J.; Alexander, C. Synthesis, Characterisation and Evaluation of Hyperbranched N-(2-Hydroxypropyl) Methacrylamides for Transport and Delivery in Pancreatic Cell Lines in Vitro and in Vivo. *Biomater. Sci.* **2022**, *10* (9), 2328–2344.

(65) Pearce, A. K.; Anane-Adjei, A. B.; Cavanagh, R. J.; Monteiro, P. F.; Bennett, T. M.; Taresco, V.; Clarke, P. A.; Ritchie, A. A.; Alexander, M. R.; Grabowska, A. M.; Alexander, C. Effects of Polymer 3D Architecture, Size, and Chemistry on Biological Transport and Drug Delivery In Vitro and in Orthotopic Triple Negative Breast Cancer Models. *Adv. Healthc. Mater.* **2020**, *9* (22), 1–14.

(66) Deng, Y.; Chen, H.; Tao, X.; Cao, F.; Trépout, S.; Ling, J.; Li, M. H. Oxidation-Sensitive Polymersomes Based on Amphiphilic Diblock Copolypeptoids. *Biomacromolecules* **2019**, *20* (9), 3435–3444.

(67) Sobotta, F. H.; Kuchenbrod, M. T.; Gruschwitz, F. V.; Festag, G.; Bellstedt, P.; Hoeppener, S.; Brendel, J. C. Tuneable Time Delay in the Burst Release from Oxidation-Sensitive

Polymersomes Made by PISA. *Angew. Chemie - Int. Ed.* **2021**, *60* (46), 24716–24723.

(68) Xu, S.; Ng, G.; Xu, J.; Kuchel, R. P.; Yeow, J.; Boyer, C. 2-(Methylthio)Ethyl Methacrylate: A Versatile Monomer for Stimuli Responsiveness and Polymerization-Induced Self-Assembly in the Presence of Air. *ACS Macro Lett.* **2017**, *6* (11), 1237–1244.

(69) De Gracia Lux, C.; Joshi-Barr, S.; Nguyen, T.; Mahmoud, E.; Schopf, E.; Fomina, N.; Almutairi, A. Biocompatible Polymeric Nanoparticles Degrade and Release Cargo in Response to Biologically Relevant Levels of Hydrogen Peroxide. *J. Am. Chem. Soc.* **2012**, *134* (38), 15758–15764.

(70) Rennick, J. J.; Johnston, A. P. R.; Parton, R. G. Key Principles and Methods for Studying the Endocytosis of Biological and Nanoparticle Therapeutics. *Nat. Nanotechnol.* **2021**, *16* (3), 266–276.

(71) Lu, F.; Wu, S. H.; Hung, Y.; Mou, C. Y. Size Effect on Cell Uptake in Well-Suspended, Uniform Mesoporous Silica Nanoparticles. *Small* **2009**, *5* (12), 1408–1413.

(72) Khetan, J.; Shahinuzzaman, M.; Barua, S.; Barua, D. Quantitative Analysis of the Correlation between Cell Size and Cellular Uptake of Particles. *Biophys. J.* **2019**, *116* (2), 347–359.

(73) Wu, M.; Guo, H.; Liu, L.; Liu, Y.; Xie, L. Size-Dependent Cellular Uptake and Localization Profiles of Silver Nanoparticles. *Int. J. Nanomedicine* **2019**, *14*, 4247–4259.

(74) Foroozandeh, P.; Aziz, A. A. Insight into Cellular Uptake and Intracellular Trafficking of Nanoparticles. *Nanoscale Res. Lett.* **2018**, *13*.

(75) Manzanares, D.; Ceña, V. Endocytosis: The Nanoparticle and Submicron Nanocompounds Gateway into the Cell. *Pharmaceutics* **2020**, *12* (4), 1–22.

(76) Ehrlich, M.; Boll, W.; Van Oijen, A.; Hariharan, R.; Chandran, K.; Nibert, M. L.; Kirchhausen, T. Endocytosis by Random Initiation and Stabilization of Clathrin-Coated Pits. *Cell* **2004**, *118* (5), 591–605.

(77) Tobias Richter, Matthias Floetenmeyer, Charles Ferguson, Janette Galea, Jaclyn Goh, Margaret R. Lindsay, Garry P. Morgan, Brad J. Marsh, R. G. P. High-Resolution 3D Quantitative Analysis of Caveolar Ultrastructure and Caveola Cytoskeleton. *Traffic* **2008**, *9*, 893–909.

Table of Contents graphic

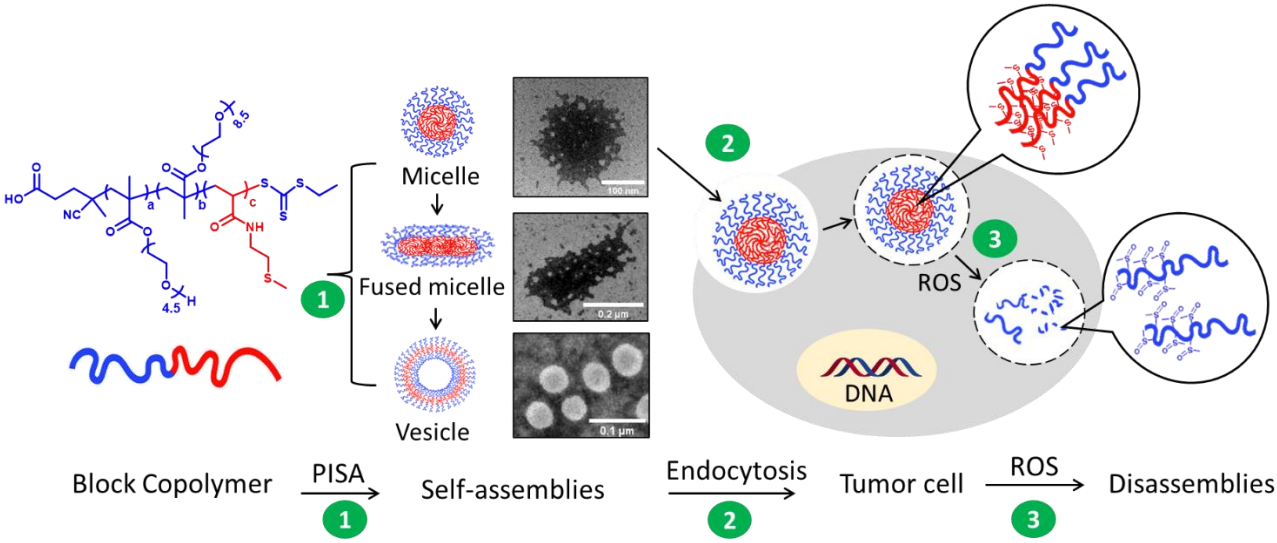

Supporting Information (SI)

H_2O_2-Responsive Nanocarriers Prepared by Reversible Addition–Fragmentation Chain Transfer-Mediated Polymerization-Induced Self-Assembly of N-(2-(Methylthio)ethyl)acrylamide for Biomedical Applications

Hien Phan,[a] *Robert Cavanagh,*[b] *Damien Destouches,*[c] *Francis Vacherot,*[c] *Blandine Brissault,*[a] *Vincenzo Taresco,*[d] *Jacques Penelle,* [a] *Benoit Couturaud* [a, *]

[a] Univ Paris Est Créteil, CNRS, Institut de Chimie et des Matériaux Paris-Est (ICMPE), UMR 7182, 2 rue Henri Dunant, 94320 Thiais, France

[b] School of Medicine, University of Nottingham, University Park, Nottingham NG7 2RD, UK

[c] Univ Paris Est Créteil, TRePCa, F-94010 Créteil, France

[d] School of Chemistry, University of Nottingham, University Park, Nottingham NG7 2RD, UK

* Corresponding author: benoit.couturaud@cnrs.fr

1. Instrumentation

1.1. Polymer characterization

Molecular weight determination of the precursor copolymers was obtained using size exclusion chromatography (SEC) in DMF as the eluent. SEC analyses were performed on a Shimadzu instrument fitted with mixed-C columns and RI. Molecular weight distributions (M_w/M_n) were calculated using poly(methyl methacrylate) (PMMA) standards. All ^1H, ^{13}C NMR spectra were recorded on a Bruker 400 MHz FT NMR spectrometer. Samples were prepared in deuterated chloroform ($CDCl_3$) and their signals referenced to residual non-deuterated signals of the solvent. The spectra were analyzed using MestReNova 12.0.4 (Mestrelab Research S.L.). Absorbance readings were performed by using UV-Vis Spectrophotometer of the Agilent Cary 60.

1.2. Particle characterization

Transmission electron microscopy (TEM)

Dry-state transmission electron microscopy (TEM) imaging was performed on either FEI TECNAI F20 microscope at an S3 acceleration voltage of 200 kV. All aqueous samples were diluted with deionized water and then deposited onto formvar-coated copper grids. Samples were directly diluted with milliQ water at the ratio of 1:100 and then deposited onto graphene oxide-coated copper grids. After roughly 1 min, excess sample was blotted from the grid and the grid was stained with an aqueous 1 wt% uranyl acetate (UA) solution for 1 min prior to blotting, drying and microscopic analysis. For determination of the average particles' size at least 100 particles were analyzed in each case.

Dynamic Light Scattering (DLS)

The intensity-average sphere equivalent diameter of diblock copolymer nano-objects was determined at 25 °C by DLS using a Malvern Zetasizer Nano S instrument via the Stokes−Einstein equation, which assumes perfectly monodisperse, non-interacting spheres. All measurements were prepared at 1 mg/mL in water. Z-average hydrodynamic diameters (D_Z) were calculated from 3 repeat measurements.

1.3. Confocal microscopy

Cells were imaged with a Zeiss LSM 700 Confocal Laser Scanning Microscope. Image J was utilized for image processing.

2. Supporting results

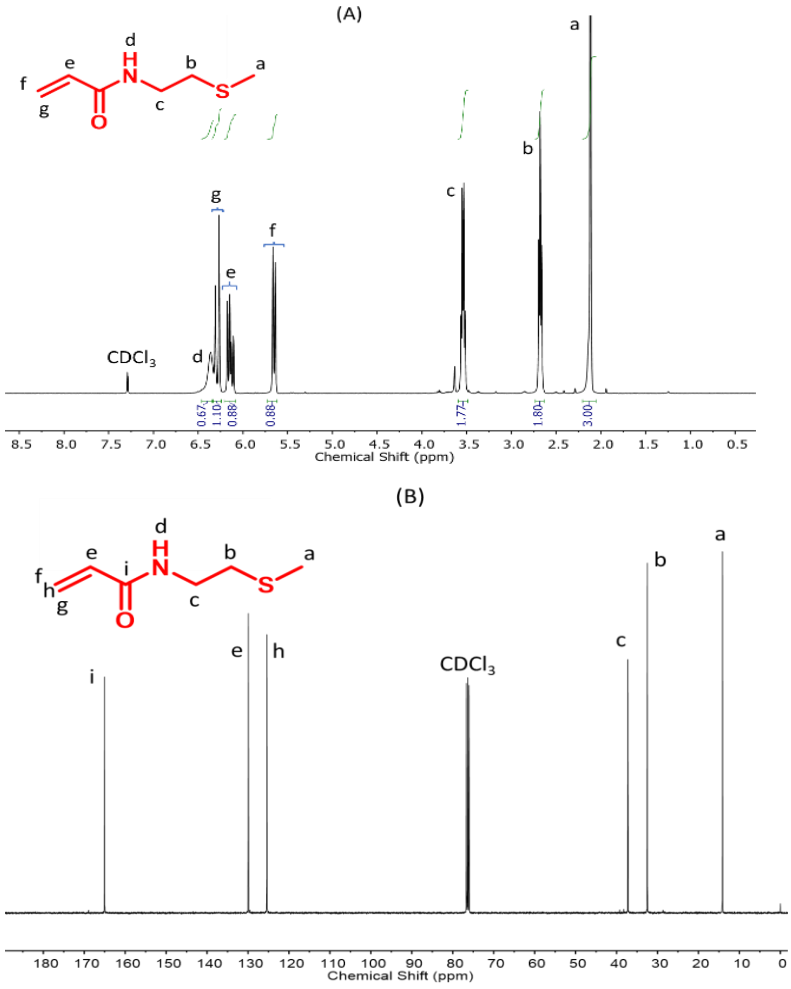

Figure S1. ^{1}H NMR (A) and ^{13}C NMR (B) of H_2O_2-sensitive MTEAM monomer in $CDCl_3$.

Table S1. Summary of results obtained from the polymerization kinetics of P-M block copolymer NPs

Time (h)	MC (%) [a]	DP [a]	Mn (kg mol^{-1}) [a]	Mn (kg mol^{-1}) [b]	$Đ$ [b]
0	NA	NA	37.42	50.91	1.48
0.25	5.13	15.40	39.66	52.90	1.64
0.5	6.22	18.66	40.13	54.55	1.60
0.75	14.91	44.72	43.92	62.19	1.79
1	36.03	108.09	53.12	77.70	1.94
2	90.32	270.98	76.77	80.76	2.57
2.5	99.11	297.33	80.60	85.95	2.60

[a] Calculated from ^{1}H NMR (DMSO), [b] SEC (PMMA standard, DMF)

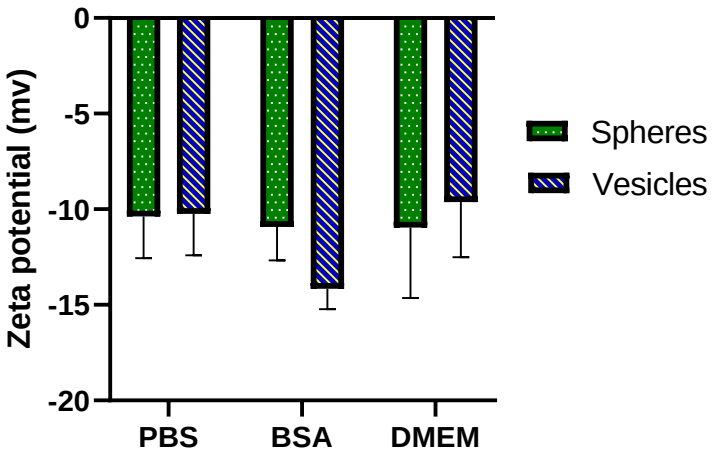

Figure S2. Zeta potential (mV) of spheres and vesicles in PBS, BSA, and DMEM after 24 h.

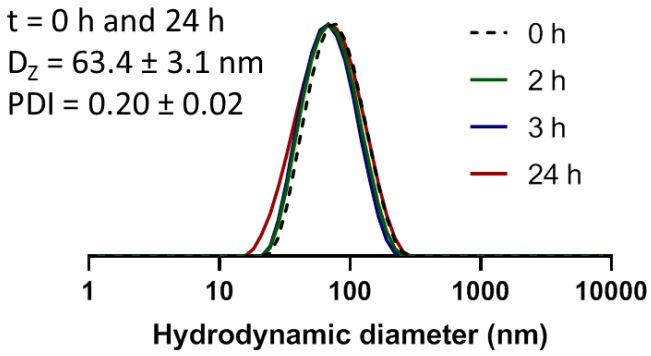

Figure S3. DLS size distributions of spherical micelles of P-M_{45} (1 mg mL^{-1}) at physiological concentration of H_2O_2 10 μM.

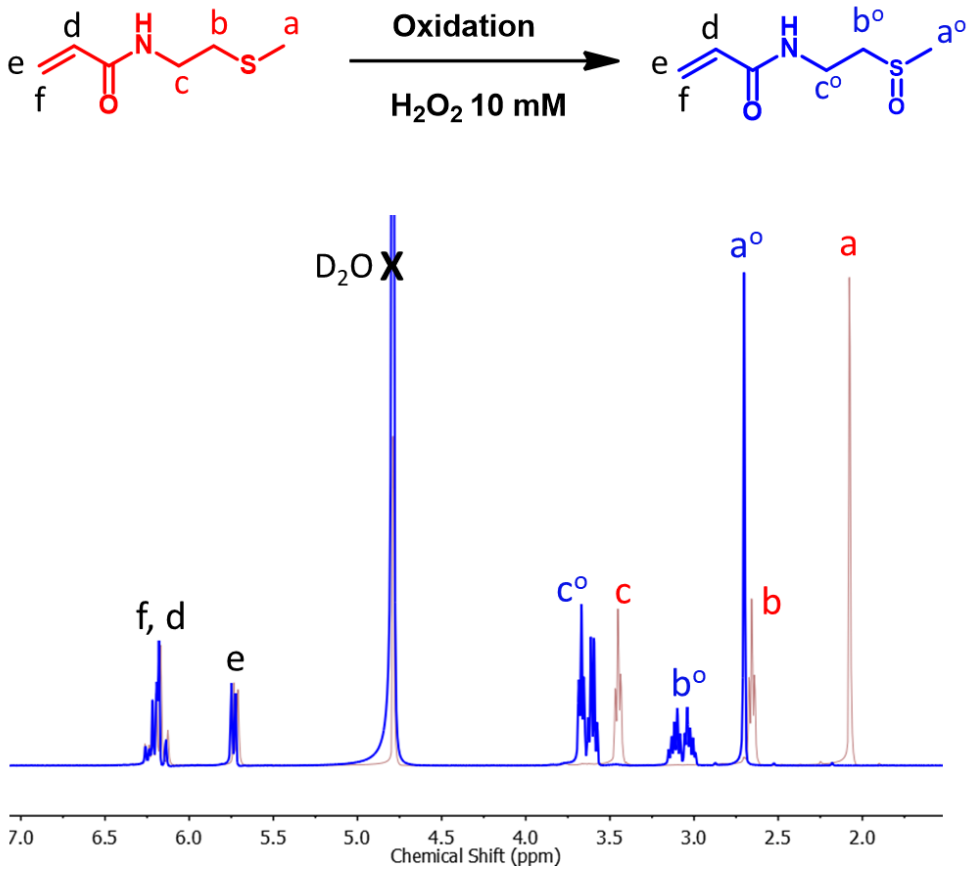

Figure S4. Merged ^{1}H NMR spectra of MTEAM monomer (red) and oxidized MTEAM monomer in H_2O_2 10 mM after 24 h (blue) in D_2O.

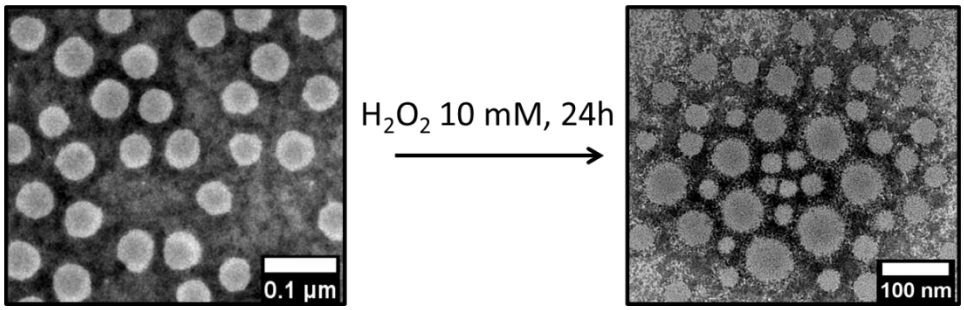

Figure S5. TEM of vesicles after incubation with H_2O_2 10 mM for 24 h.

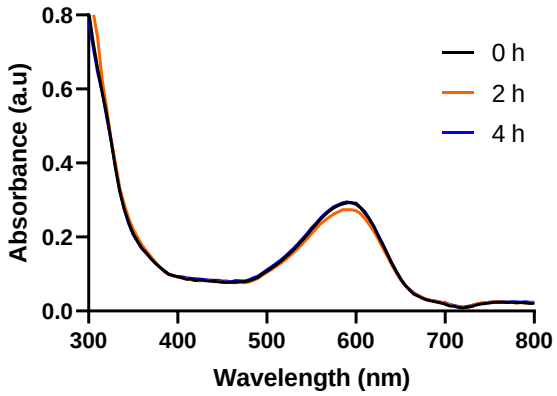

Figure S6. Uv-Vis spectra of NR-loaded NP in PBS.

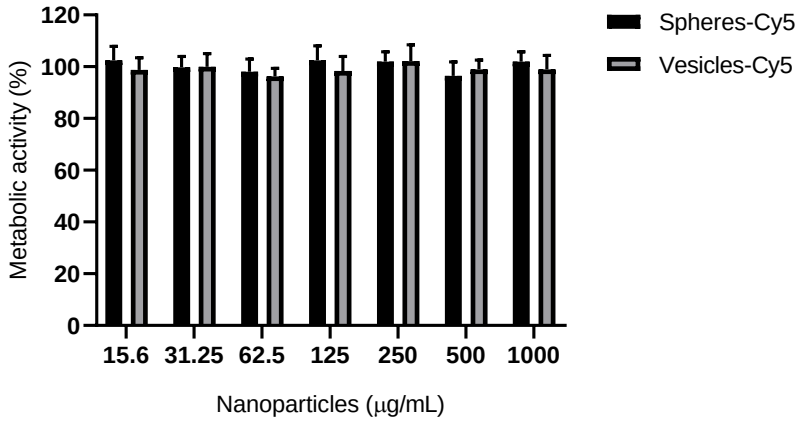

Figure S7. Cell viability of spheres-Cy5 and vesicles-Cy5 in MCF-7 cells. Cytotoxicity was determined by the PrestoBlue viability assay. NPs incubated for 24 h on cells and applied in complete DMEM medium. Data are presented as mean ± SD (n = 3).

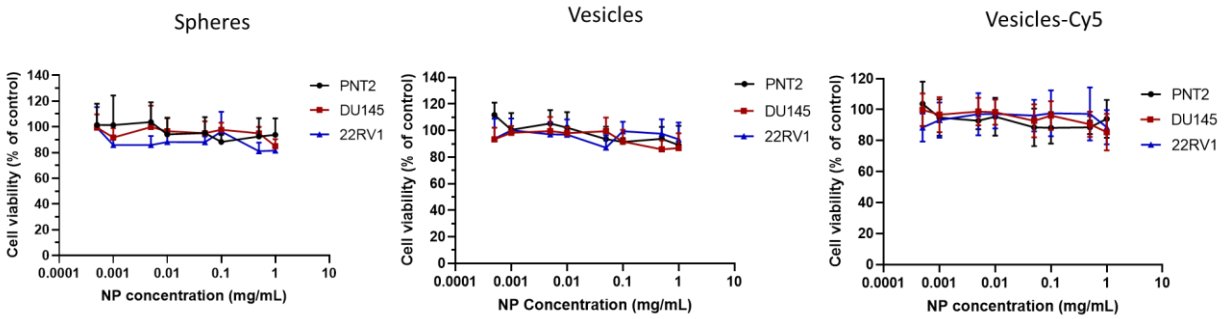

Figure S8. Cell viability of spheres, vesicles, and vesicles-Cy5 in three prostate cell lines (PNT-2, DU145, 22RV1.) Cytotoxicity was determined by the MTT viability assay. NPs incubated for 72 h on cells. Data are presented as mean ± SD (n = 8).